

# Role of Oxido Incorporation and Ligand Lability in Expanding Redox Accessibility of Structurally Related Mn<sub>4</sub> Clusters

Jacob S. Kanady,<sup>a</sup> Rosalie Tran,<sup>b</sup> Jamie A. Stull,<sup>c</sup> Luo Lu,<sup>c</sup> Troy A. Stich,<sup>c</sup> Michael W. Day,<sup>a</sup> Junko Yano,<sup>b\*</sup> R. David Britt,<sup>c\*</sup> and Theodor Agapie<sup>a\*\*</sup>

## Supporting Online Material

### Contents

<b>General Considerations</b>	S1
<b>Synthetic Procedures</b>	S2
<b>Figure S1</b> <sup>1</sup> H NMR spectrum of <b>2</b>	S4
<b>Figure S2</b> <sup>1</sup> H NMR spectra of <b>2</b> comparing Methods A and B	S5
<b>Figure S3</b> <sup>1</sup> H NMR spectrum of <b>3</b>	S5
<b>Figure S4</b> <sup>1</sup> H NMR spectrum of <b>4</b>	S6
<b>Figure S5</b> <sup>1</sup> H NMR spectra of <b>6</b>	S6
<b>Figure S6</b> <sup>1</sup> H NMR spectrum of <b>7</b>	S7
<b>Cyclic Voltammetry</b>	S7
<b>Figure S7</b> Cyclic Voltammogram of <b>3</b> in CH <sub>2</sub> Cl <sub>2</sub>	S7
<b>XAS Methods</b>	S8
<b>Table S1</b> Mn K-edge EXAFS curve-fitting parameters for complexes <b>3-6</b>	S9
<b>Figure S8</b> Fourier transforms of the Mn EXAFS for complexes <b>3-6</b>	S10
<b>EPR Methods</b>	S10
<b>Figure S9</b> X-band EPR of complex <b>6</b> with simulation	S11
<b>Magnetism Studies</b>	S11
<b>Figure S10</b> Exchange coupling models	S12
<b>Crystallographic Information</b>	S12
<b>Table S2</b> Crystal and refinement data	S13
<b>References</b>	S14

### General Considerations

Reactions performed under inert atmosphere were carried out in a glovebox under a nitrogen atmosphere. Anhydrous tetrahydrofuran (THF) was purchased from Aldrich in 18 L Pure-Pac<sup>TM</sup> containers. Anhydrous dichloromethane, diethyl ether, and THF were purified by sparging with nitrogen for 15 minutes and then passing under nitrogen pressure through a column of activated A2 alumina (Zapp's). Anhydrous *N,N*-dimethylformamide (DMF) was purchased from Aldrich and stored over molecular sieves. NMR solvents were purchased from Cambridge Isotope Laboratories, Inc. CD<sub>2</sub>Cl<sub>2</sub> was dried over calcium hydride, then degassed by three freeze-pump-thaw cycles and vacuum-transferred prior to use. <sup>1</sup>H NMR and <sup>13</sup>C NMR spectra were recorded on a Varian 300 MHz instrument, with shifts reported relative to the residual solvent peak. Elemental analyses were performed by Midwest Microlab, LLC, Indianapolis, IN. High-resolution mass spectrometry (HRMS) was performed at the California Institute of Technology Mass Spectra Facility.

Unless indicated otherwise, all commercial chemicals were used as received. Tetrabutylammonium permanganate,<sup>1</sup> iodosobenzene,<sup>2</sup> and Mn(OTf)<sub>2</sub>•CH<sub>3</sub>CN<sup>3</sup> were prepared

according to literature procedures. **Caution!** Tetrabutylammonium permanganate and iodosobenzene are potentially explosive and should be used only in small quantities.

### Synthetic Procedures

**Synthesis of 1,3,5-Tris(2-di(2'-pyridyl)hydroxymethylphenyl)benzene (H<sub>3</sub>L):** An improved synthesis was described in a past publication.<sup>4</sup>

**Synthesis of LMn<sup>II</sup><sub>3</sub>(OAc)<sub>3</sub> (1).** An improved synthesis was described in a past publication.<sup>4</sup>

**Synthesis of LMn<sup>II</sup><sub>3</sub>Mn<sup>III</sup>O<sub>1</sub>(OAc)<sub>4</sub> (2).** Method A from 1: In the glovebox, yellow solid **1**•CHCl<sub>3</sub> (42 mg, 0.03 mmol) was suspended in THF (5 mL). Mn(OAc)<sub>2</sub> (5.8 mg, 0.03 mmol) was added as a solid, followed by KO<sub>2</sub> (4.5 mg, 0.06 mmol). The heterogeneous mixture slowly became brown. After magnetically stirring for 4 days, the solution was brown with brown precipitate. The brown solid was collected on a frit with a bed of celite, rinsed with THF (~10 mL), the THF fraction was discarded, and the solid was solubilized and rinsed through with CH<sub>2</sub>Cl<sub>2</sub>. The resulting red-brown solution was concentrated *in vacuo* to afford brown solid **2** (30 mg, 70%). Recrystallization from vapor diffusion of Et<sub>2</sub>O into a DMF solution gave crystals amenable to X-ray diffraction studies.

Method B from 3: In the glovebox, the purple solid **3** (126.3 mg, 0.08 mmol) was dissolved in CH<sub>2</sub>Cl<sub>2</sub> (8 mL). Decamethylferrocene (27.6 mg, 0.085 mmol) was added to the purple-brown solution of **3** as an orange solution in CH<sub>2</sub>Cl<sub>2</sub> (1 mL). The reaction mixture turned gray-brown. Volatile materials were removed *in vacuo* after 30 minutes of stirring. The resulting solid was dissolved in minimal CH<sub>3</sub>CN and Et<sub>2</sub>O was allowed to vapor diffuse into the solution to afford large green crystals ([FeCp\*]OTf) and small purple crystals. The crystals were separated manually to afford 60 mg of purple, crystalline material. Based on preliminary XRD studies and elemental analysis, this material was characterized as dimeric [LMn<sup>II</sup><sub>3</sub>Mn<sup>III</sup>O<sub>1</sub>(OAc)<sub>3</sub>]<sub>2</sub>•2OTf: Anal. Calcd. for C<sub>128</sub>H<sub>96</sub>F<sub>6</sub>Mn<sub>8</sub>N<sub>12</sub>O<sub>26</sub>S<sub>2</sub>: C, 54.21; H, 3.41; N, 5.93. Found: C, 54.29; H, 3.63; N, 5.86. A sample of this material (27 mg, 0.01 mmol) was dissolved in CH<sub>3</sub>CN (3 mL), and a solution of <sup>181</sup>Bu<sub>4</sub>NOAc (16 mg, 0.05 mmol) in CH<sub>3</sub>CN (1 mL) was added. Within seconds, a brown precipitate formed. The mixture was allowed to stir for 15 minutes and then filtered through Celite. The brown solid was rinsed with ample CH<sub>3</sub>CN. The solid was washed through with CH<sub>2</sub>Cl<sub>2</sub> and volatiles were removed *in vacuo* to afford brown solid **2**. (16.2 mg, 34% from **3**). <sup>1</sup>H NMR (300 MHz, CD<sub>2</sub>Cl<sub>2</sub>, 25 °C) 42.1 (Δν<sub>1/2</sub>=1500 Hz), 38.3 (Δν<sub>1/2</sub>=700 Hz), 31.9 (Δν<sub>1/2</sub>=240 Hz), 11.3 (Δν<sub>1/2</sub>=180 Hz), 8.6 (Δν<sub>1/2</sub>=460 Hz), 5.0 (Δν<sub>1/2</sub>=180 Hz), -4.2 (Δν<sub>1/2</sub>=220 Hz), -7.5 (Δν<sub>1/2</sub>=330 Hz) ppm. UV-Vis (λ<sub>max</sub> [ε (M<sup>-1</sup> cm<sup>-1</sup>)]): 254 (5.2x10<sup>4</sup>), 418 (720), 491 (520) nm. Anal. Calcd. for C<sub>66</sub>H<sub>53</sub>Cl<sub>2</sub>Mn<sub>4</sub>N<sub>6</sub>O<sub>12</sub> (**3**•CH<sub>2</sub>Cl<sub>2</sub>): C, 56.11; H 3.78; N, 5.95. Found: C, 56.67; H, 3.90; N, 5.98.

**Synthesis of [LMn<sup>II</sup><sub>2</sub>Mn<sup>III</sup><sub>2</sub>O<sub>1</sub>(OAc)<sub>3</sub>(OTf)]OTf (3).** In the glovebox, the yellow solid **1**•THF (523 mg, 0.41 mmol) was suspended in THF (80 mL) and Mn(OTf)<sub>2</sub>•CH<sub>3</sub>CN (170 mg, 0.43 mmol) was separately dissolved in THF (20 mL). The solution of Mn(OTf)<sub>2</sub> was added by pipette to the suspension of **1**, affording a ~4mM solution of **1**. Iodosobenzene (90 mg, 0.41 mmol) was added as a solid to this hazy, yellow solution. The heterogeneous solution turned purple, then brown and mostly homogeneous within 30 minutes at which point a brown precipitate formed. After stirring for 1 hour, the mixture was filtered through Celite to afford a purple solid and brown solution. The solid was rinsed with some THF and then rinsed through with CH<sub>2</sub>Cl<sub>2</sub>. Both fractions were concentrated *in vacuo* to give brown-purple powder. The powder from the THF fraction was triturated in benzene, collected by filtration, and rinsed with

~40 mL benzene to remove iodobenzene. The resulting solid **3** was pure by  $^1\text{H}$  NMR (410 mg, 64%). The powder from the  $\text{CH}_2\text{Cl}_2$  fraction—ca. 95% pure by  $^1\text{H}$  NMR—was recrystallized from vapor diffusion of  $\text{Et}_2\text{O}$  into  $\text{CH}_3\text{CN}$  to afford pure **3** (180 mg, 28%, 91% total yield). Recrystallization from vapor diffusion of  $\text{Et}_2\text{O}$  into a  $\text{CH}_2\text{Cl}_2$ /dimethoxyethane solution gave crystals amenable to X-ray diffraction studies.  $^1\text{H}$  NMR (300 MHz,  $\text{CD}_2\text{Cl}_2$ , 25 °C) 45.3 ( $\Delta\nu_{1/2}=800$  Hz), 40.8 ( $\Delta\nu_{1/2}=410$  Hz), 35.5 & 33.3 (overlapping), 11.5 ( $\Delta\nu_{1/2}=100$  Hz), 8.1 ( $\Delta\nu_{1/2}=160$  Hz), 7.1 ( $\Delta\nu_{1/2}=650$  Hz), 5.2 ( $\Delta\nu_{1/2}=90$  Hz), -9.2 ( $\Delta\nu_{1/2}=220$  Hz), -11.5 ( $\Delta\nu_{1/2}=230$  Hz) ppm.  $^{19}\text{F}$  NMR (282 MHz,  $\text{CD}_2\text{Cl}_2$ , 25 °C): 60.0 ( $\Delta\nu_{1/2}=750$  Hz) ppm. UV-Vis ( $\lambda_{\text{max}}$  [ $\epsilon$  ( $\text{M}^{-1}\text{cm}^{-1}$ )]): 251 ( $5.4\times 10^4$ ), 412 (870), 489 (810) nm. Anal. Calcd. for  $\text{C}_{65}\text{H}_{48}\text{F}_6\text{Mn}_4\text{N}_6\text{O}_{16}\text{S}_2$ : C, 49.82; H, 3.09; N, 5.36. Found: C, 50.09; H, 3.45; N, 5.44.

**Synthesis of  $\text{LMn}^{\text{II}}_2\text{Mn}^{\text{III}}_2\text{O}_2(\text{OAc})_3$  (**4**).** In the glovebox, yellow solid **1**•THF (365 mg, 0.28 mmol) was suspended in  $\text{CH}_3\text{CN}$  (18 mL) and  $\text{Mn}(\text{OAc})_2$  (50.3 mg, 0.29 mmol) was added as a solid.  $\text{KO}_2$  (59.0 mg, 0.83 mmol) was then added as a solid, and the heterogeneous mixture was magnetically stirred for 3.5 days to afford a tan precipitate and green/brown solution. The precipitate was collected by filtration over Celite, washed with  $\text{CH}_3\text{CN}$ , and then rinsed through with  $\text{CH}_2\text{Cl}_2$ .  $\text{CH}_2\text{Cl}_2$  was removed *in vacuo*, affording an analytically pure tan powder **4** (225 mg, 63%). Recrystallization from vapor diffusion of  $\text{Et}_2\text{O}$  into a DMF solution gave crystals amenable to X-ray diffraction studies.  $^1\text{H}$  NMR (300 MHz,  $\text{CD}_2\text{Cl}_2$ , 25 °C) 61.9 ( $\Delta\nu_{1/2}=900$  Hz), 54.0 ( $\Delta\nu_{1/2}=1350$  Hz), 46.3 ( $\Delta\nu_{1/2}=720$  Hz), 42.3 & 40.8 (overlapping), 30.8 ( $\Delta\nu_{1/2}=340$  Hz), 20.4 & 19.7 (overlapping), 11.9 ( $\Delta\nu_{1/2}=130$  Hz), 11.1 ( $\Delta\nu_{1/2}=420$  Hz), 8.6 & 7.7 (overlapping), 6.3 ( $\Delta\nu_{1/2}=200$  Hz), 4.0 ( $\Delta\nu_{1/2}=290$  Hz), -4.1 ( $\Delta\nu_{1/2}=370$  Hz), -7.8 ( $\Delta\nu_{1/2}=350$  Hz), -15.2 & -16.0 (overlapping) ppm. All resonances are paramagnetically broadened. UV-Vis ( $\lambda_{\text{max}}$  [ $\epsilon$  ( $\text{M}^{-1}\text{cm}^{-1}$ )]): 254 ( $8.0\times 10^4$ ) nm. Anal. Calcd. for  $\text{C}_{63}\text{H}_{48}\text{Mn}_4\text{N}_6\text{O}_{11}$ : C, 58.89; H, 3.77; N, 6.54. Found: C, 58.58; H, 3.86; N, 6.31.

**Synthesis of  $\text{LMn}^{\text{III}}_4\text{O}_3(\text{OAc})_3$  (**5**).** Both methods of synthesis (either from **1** or **6**) are detailed in a recent publication.<sup>4</sup>

**Synthesis of  $\text{LMn}^{\text{III}}_2\text{Mn}^{\text{IV}}_2\text{O}_4(\text{OAc})_3$  (**6**).** Three methods for synthesis of **6** (from **1**,<sup>5</sup> from **5** and PhIO,<sup>4</sup> and from **5**,  $\text{NR}_4\text{OH}$  and  $\text{FcPF}_6$ )<sup>4</sup> are detailed in past publications.

Method from **4** and  $\text{O}_2$ : In the glovebox, **4** (50 mg, 0.04 mmol, 200  $\mu\text{M}$ ) was dissolved in DMF (200 mL) in an oven-dried schlenk tube to give a brown and clear solution. The schlenk tube was brought out of the glovebox, connected to the schlenk line, and degassed by introducing the solution to vacuum with vigorous stirring for ~2 min. An atmosphere of  $\text{O}_2$  was introduced with vigorous stirring for ~2min, and the degassing/ $\text{O}_2$ -introduction cycle was repeated four times. Aliquots (~25 mL each) for  $^1\text{H}$  NMR analysis were removed by syringe, transferred to an oven-dried schlenk tube, and concentrated *in vacuo* to give brown solids. After six aliquots over 12 days, the remaining reaction mixture (~ 50 mL) was concentrated *in vacuo* to give the final sample at 13 days (~60% **6** by  $^1\text{H}$  NMR).

Spectral features match those found in previous work.<sup>4, 5</sup>

**Synthesis of  $[\text{LMn}^{\text{III}}_2\text{Mn}^{\text{IV}}_2\text{O}_4(\text{OAc})_2(3,5\text{-dimethylpyrazole})_2]\text{OTf}$  (**7**):** In the glovebox, **6** (71.6 mg, .055 mmol) was dissolved in  $\text{CH}_2\text{Cl}_2$ . While stirring the solution of **6**,  $\text{Me}_3\text{SiOTf}$  was added as a 0.1M solution in  $\text{CH}_2\text{Cl}_2$  (0.57 ml, 0.057 mmol, 1.05 equiv) dropwise. The solution was stirred magnetically for 30 minutes, and then volatiles were removed *in vacuo*. The resulting brown residue was washed with hexanes to remove  $\text{Me}_3\text{SiOAc}$  byproduct. The residue was then dissolved in  $\text{C}_6\text{H}_6$  and filtered through celite, leaving some brown solid that was discarded. The

brown C<sub>6</sub>H<sub>6</sub> solution was concentrated *in vacuo* to dryness, affording LMn<sub>4</sub>O<sub>4</sub>(OAc)<sub>2</sub>(OTf) (72 mg, 90%). A sample of this material (51.5 mg, 0.037 mmol) was dissolved in C<sub>6</sub>H<sub>6</sub> (6 mL) and 3,5-dimethylpyrazole (27.0 mg, 0.3 mmol, 8 equiv) was added as a solid. The solution was stirred magnetically for 40 minutes, and then solvent was removed *in vacuo*. The resulting residue was triturated in hexanes, collected on celite, and rinsed with 8 ml hexanes to remove excess 3,5-dimethylpyrazole. The brown solid was rinsed through with CH<sub>2</sub>Cl<sub>2</sub> and volatiles were removed *in vacuo*. Microcrystalline precipitate **7** was isolated by Et<sub>2</sub>O vapor diffusion into a 1:1 CH<sub>2</sub>Cl<sub>2</sub>/C<sub>6</sub>H<sub>6</sub> solution (20 mg, 34%). X-ray quality crystals were grown from Et<sub>2</sub>O vapor diffusion into a C<sub>6</sub>H<sub>6</sub> solution of **7**. <sup>1</sup>H NMR (300 MHz, CD<sub>2</sub>Cl<sub>2</sub>, 25 °C) 26.6, 25.7, 22.5, 21.1, 18.1, 15.4 (overlapping), 10.4, 9.1, 8.8, 8.2, 7.6, 7.1 (overlapping), 6.1, 5.3, 4.8, 4.3, 2.7 (overlapping), -14.2, -14.7 ppm (overlapping). <sup>19</sup>F NMR (282 MHz, CD<sub>2</sub>Cl<sub>2</sub>, 25 °C) -76.4 ppm. UV-Vis (λ<sub>max</sub> [ε (M<sup>-1</sup> cm<sup>-1</sup>)]): 238 (9.3x10<sup>4</sup>), 310 (2.3x10<sup>4</sup>), 715 (200) nm. Anal. Calcd. for C<sub>79</sub>H<sub>69</sub>Cl<sub>2</sub>F<sub>3</sub>Mn<sub>4</sub>N<sub>10</sub>O<sub>14</sub>S (**7**• CH<sub>2</sub>Cl<sub>2</sub>•C<sub>6</sub>H<sub>6</sub>) (sample crystallized from CH<sub>2</sub>Cl<sub>2</sub>/C<sub>6</sub>H<sub>6</sub>): C, 53.85; H, 3.95; N, 7.95. Found: C, 53.72; H, 4.05; N, 7.73.

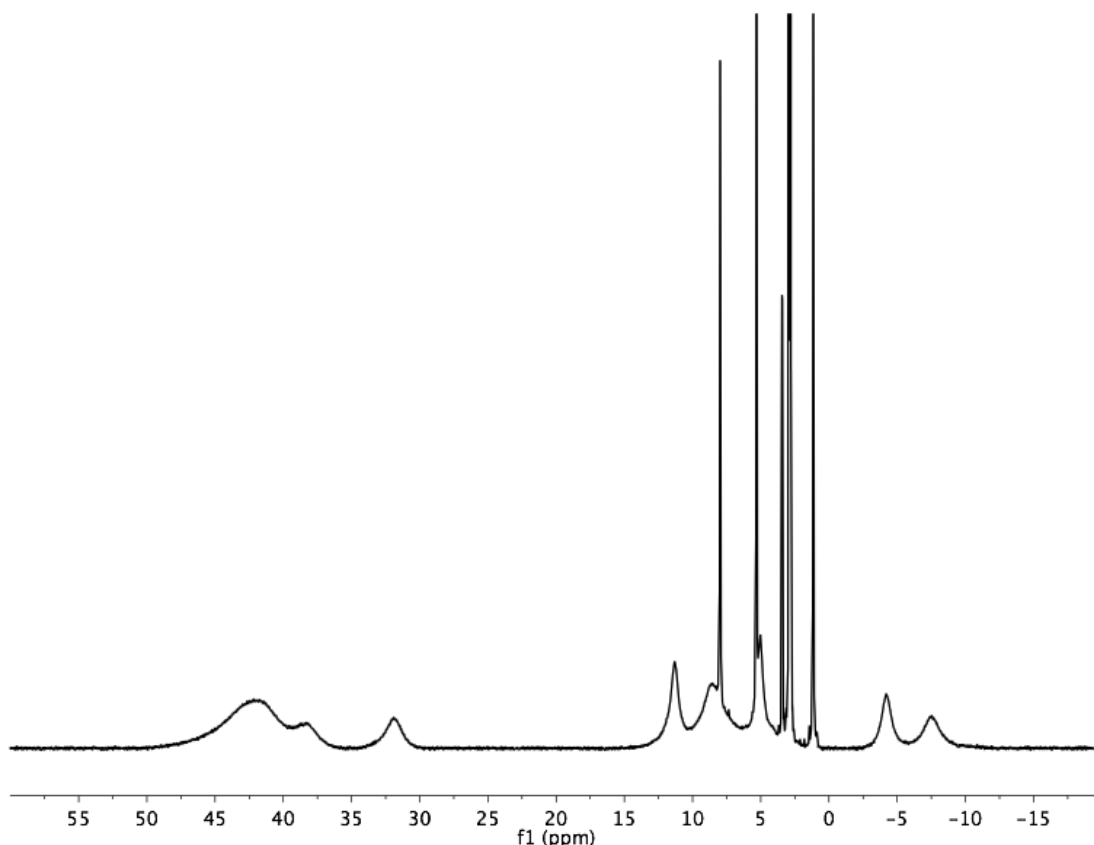
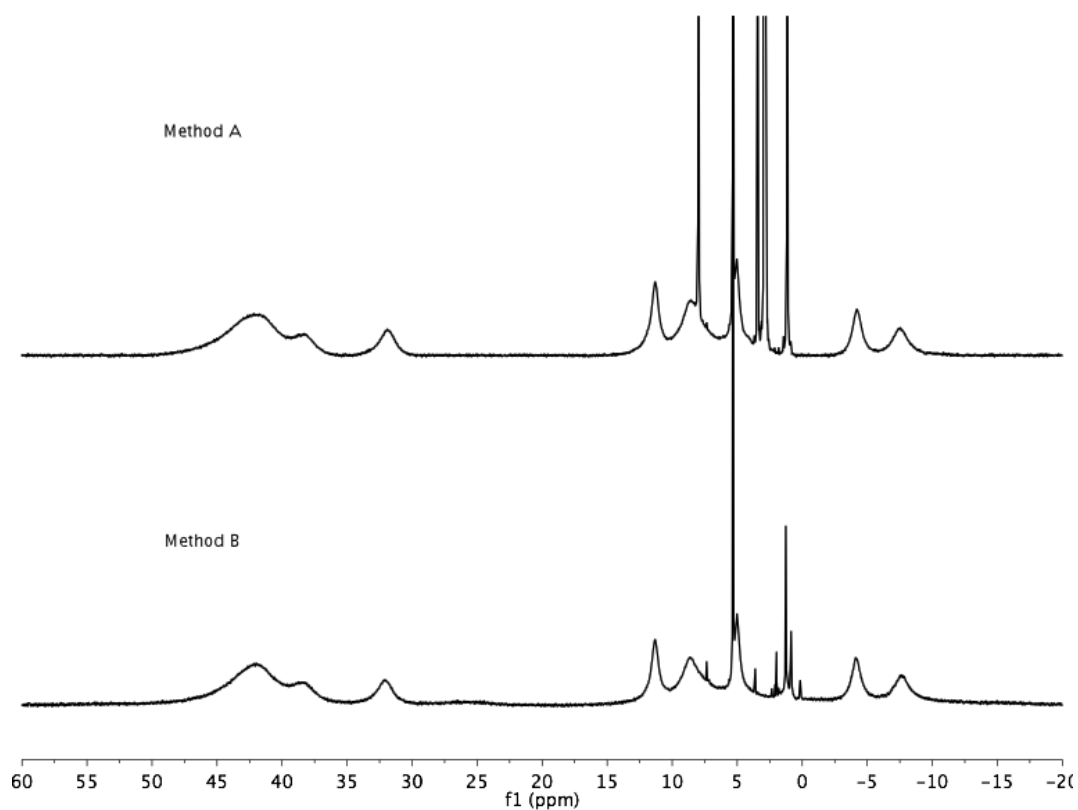
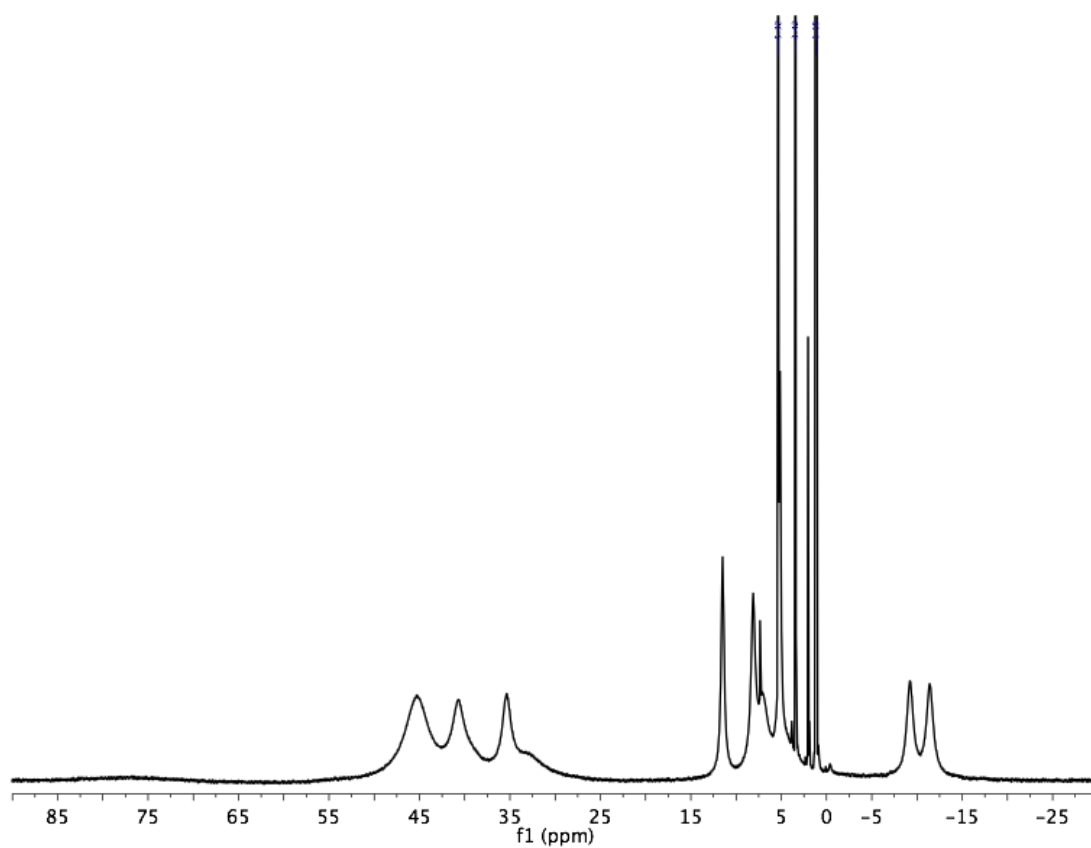


Figure S1. <sup>1</sup>H NMR spectrum of **2** in CD<sub>2</sub>Cl<sub>2</sub> at 25 °C.



**Figure S2.** <sup>1</sup>H NMR spectrum of **2** synthesized from Methods A and B in CD<sub>2</sub>Cl<sub>2</sub> at 25 °C.



**Figure S3.** <sup>1</sup>H NMR spectrum of **3** in CD<sub>2</sub>Cl<sub>2</sub> at 25 °C.

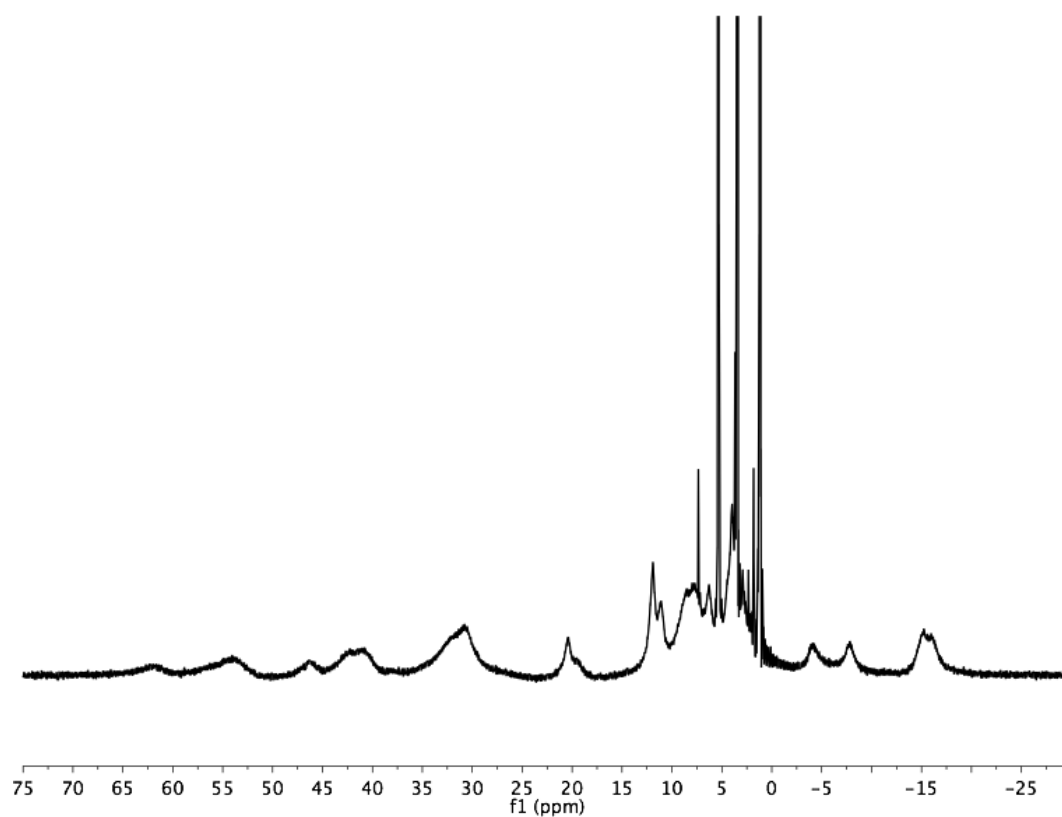


**Figure S4.** <sup>1</sup>H NMR spectrum of **4** in CD<sub>2</sub>Cl<sub>2</sub> at 25 °C.

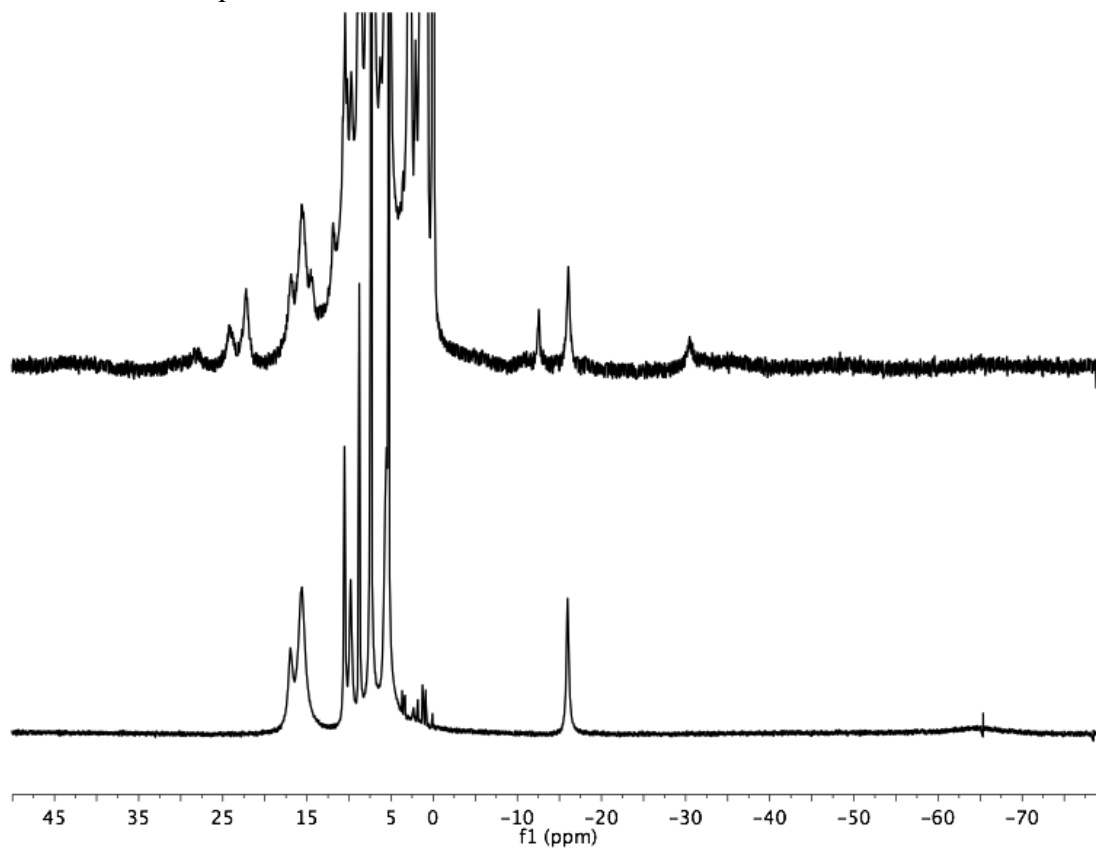


**Figure S5.** <sup>1</sup>H NMR spectra of **6** both purified (bottom) and synthesized from **4** and O<sub>2</sub> (top) in CD<sub>2</sub>Cl<sub>2</sub> at 25 °C.

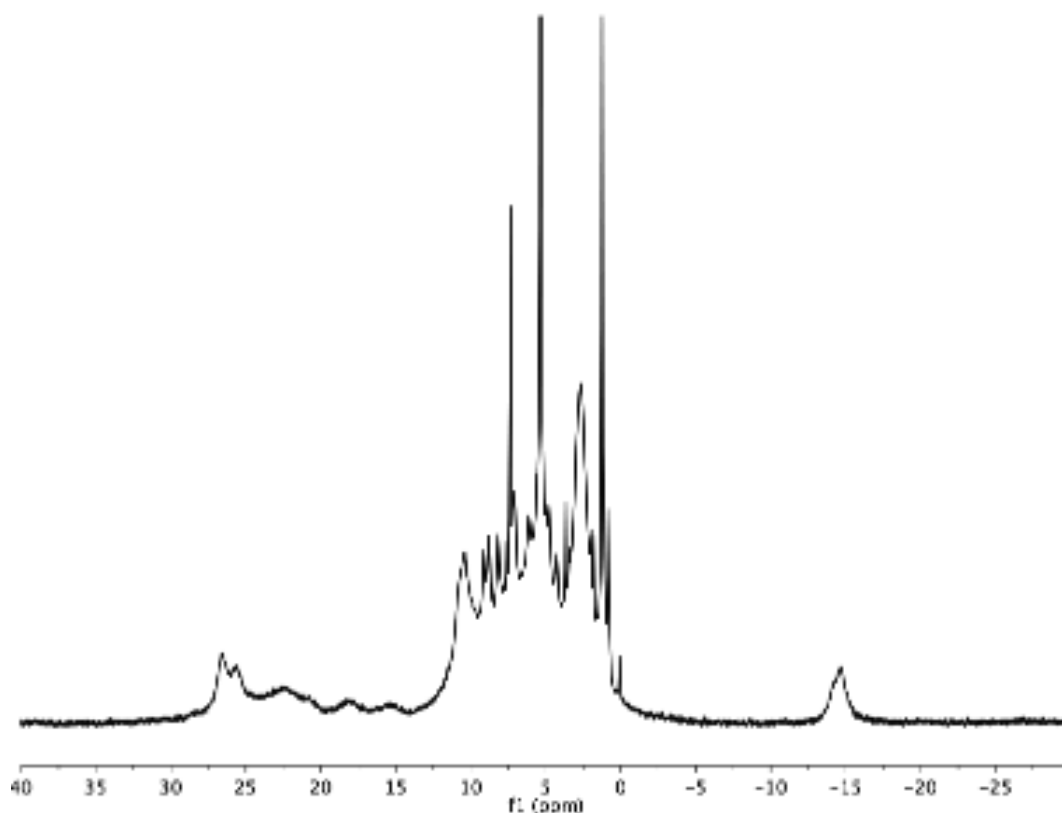


**Figure S6.**  $^1\text{H}$  NMR spectra of **7** in  $\text{CD}_2\text{Cl}_2$  at 25 °C.

#### *Cyclic Voltammetry*

Electrochemical measurements were recorded under a nitrogen atmosphere in a MBraun glovebox at 25 °C with a Pine Instrument Company AFCBP1 bipotentiostat. An auxiliary Pt-coil electrode, a  $\text{Ag}/\text{Ag}^+$  reference electrode (0.01 M  $\text{AgNO}_3$  in  $\text{CH}_3\text{CN}$ ), and a 3.0 mm glassy carbon electrode disc (BASI) were used. Data were recorded using the Pine Instrument Company AfterMath software package. All reported values were referenced to an internal ferrocene/ferrocenium couple. The electrolyte solutions were 0.1 M  $n\text{Bu}_4\text{NPF}_6$  in  $\text{CH}_2\text{Cl}_2$  in the study of **3** and 0.1M  $n\text{Bu}_4\text{NPF}_6$  in THF for **5**, **6** and **7**.

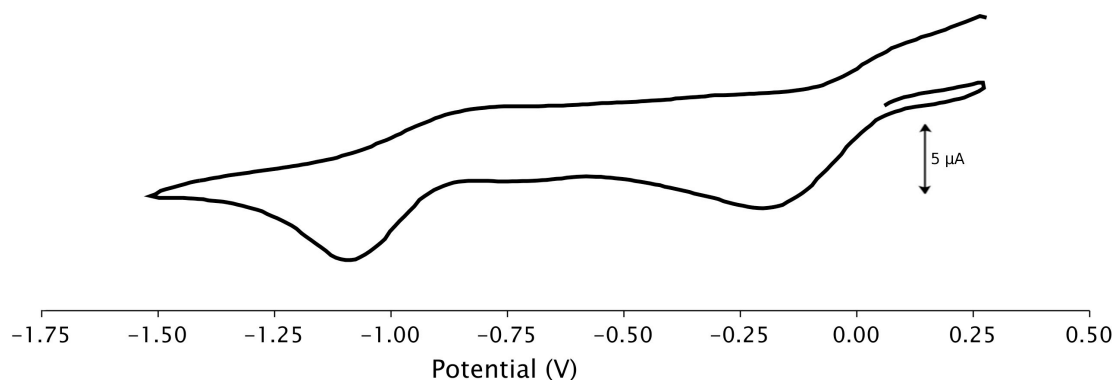


**Figure S7.** Cyclic voltammogram of **3** referenced to  $\text{Fc}/\text{Fc}^+$ . The scan rate was 100 mV/s initially in the positive direction. The analyte concentration was 1.0 mM. The electrolyte was 0.1M  $n\text{Bu}_4\text{NPF}_6$  in  $\text{CH}_2\text{Cl}_2$ . Open-circuit potential was 70 mV.  $E_{\text{cat}}$  values: -0.2 V assigned to  $\text{Mn}^{\text{II}}_2\text{Mn}^{\text{III}}_2/\text{Mn}^{\text{II}}_3\text{Mn}^{\text{III}}$  and -1.0 V assigned to  $\text{Mn}^{\text{II}}_3\text{Mn}^{\text{III}}/\text{Mn}^{\text{II}}_4$ .

## XAS Methods

**Mn X-ray Absorption Spectroscopy (XAS) Data Collection.** XAS measurements were performed at the Stanford Synchrotron Radiation Laboratory on Beamline 7-3 at an electron energy of 3.0 GeV with an average current of 350 mA. The radiation was monochromatized by a Si(220) double-crystal monochromator. An N<sub>2</sub>-filled ion chamber (I<sub>0</sub>) in front of the sample was used to monitor the intensity of the incident X-ray beam. A Ge 30-element detector (Canberra) was used to collect the data as fluorescence excitation spectra. The monochromator energy was calibrated using the pre-edge peak of KMnO<sub>4</sub> (6543.3 eV). The calibration standard was placed between two N<sub>2</sub>-filled ionization chambers (I<sub>1</sub> and I<sub>2</sub>) after the sample. The X-ray flux at 6.6 keV ranged from 2 to 5 × 10<sup>9</sup> photons s<sup>-1</sup>mm<sup>-2</sup> of the sample. To minimize radiation damage, samples were maintained at a temperature of 10 K in a liquid He flow cryostat.

To prepare the XAS samples, 5-10 mg of the individual complexes were finely ground with a mortar and pestle in a glovebox, and diluted with boron nitride (1% w/w). The mixture was packed anaerobically into 0.5 mm thick aluminum sample holders and sealed with Kapton tape. To ensure that no X-ray induced radiation damage occurred, the Mn K-edge was closely monitored for any reduction of manganese as seen by a shift in the K-edge inflection point energy.

### Data reduction and analysis for EXAFS

Data reduction of the EXAFS spectra was performed using SamView (SixPACK software, Dr. Samuel M. Webb, SSRL). The pre-edge and post-edge backgrounds were subtracted from the XAS spectra using Athena (IFEFFIT software,<sup>6, 7</sup>), and the resulting spectra were normalized with respect to the edge height. The background removal in *k*-space was performed using a cubic spline function. Curve fitting was performed with Artemis and IFEFFIT software using *ab initio* calculated phases and amplitudes from the program FEFF 8.2.<sup>6, 7</sup> These *ab initio* calculated phases and amplitudes were applied in the EXAFS equation:

$$\chi(k) = S_0^2 \sum_j \frac{N_j}{kR_j^2} f_{eff}(\pi, k, R_j) e^{-2\sigma_j^2 k^2} e^{-2R_j/\lambda_j(k)} \sin[2kR_j + \phi_{ij}(k)] \quad [\text{Eq. 1}]$$

where the neighboring atoms to the central atom(s) are divided into *j* shells, with all atoms having the same atomic number and distance from the central atom(s) grouped into a single shell. For each shell, the coordination number *N<sub>j</sub>* indicates the number of neighboring atoms in shell *j* at a distance of *R<sub>j</sub>* from the central atom(s). *f<sub>eff</sub>*(*π, k, R<sub>j</sub>*) defines the *ab initio* amplitude function for shell *j*, and the Debye-Waller term *e<sup>-2σ<sub>j</sub><sup>2</sup>k<sup>2</sup></sup>* denotes the damping that occurs due to static and thermal disorder in absorber-scatterer distances. Losses due to inelastic scattering are defined by the mean free path term, *e<sup>-2R<sub>j</sub>/λ<sub>j</sub>(k)</sup>*, where the electron mean free path is denoted as *λ<sub>j</sub>(k)*. The sinusoidal term, *sin[2kR<sub>j</sub> + φ<sub>ij</sub>(k)]*, represents the oscillations in the EXAFS spectrum, where *φ<sub>ij</sub>(k)* is the *ab initio* phase function for shell *j*. The term *S<sub>0</sub><sup>2</sup>* is the amplitude reduction factor due to shake-up/shake-off processes that occur at the central atom(s). This EXAFS equation was used to fit the experimental data using *N*, *R*, and the EXAFS Debye-Waller factor (*σ<sup>2</sup>*) as variable parameters. For the energy (eV) to wave vector (*k*, Å<sup>-1</sup>) axis conversion, *E<sub>0</sub>* was defined as 6561.3 eV.

**Table S1:** Mn K-edge EXAFS curve-fitting parameters for complexes **3-6**.<sup>a</sup>

Complex	Path	R (Å)		N	$\sigma^2$ (Å <sup>2</sup> )	R (%)
		EXAFS	XRD			
<b>3</b>	Mn-O	1.99 (0.03)	1.93–2.29	<b>3.5</b>	0.014 (0.005)	1.4
	Mn-O	2.18 (0.08)		<b>0.75</b>	0.002 (0.002)	$\Delta E_0 = -10.6$
	Mn-N	2.19 (0.04)	2.13–2.31	<b>1.5</b>	0.002 (0.002)	
	Mn-C	2.97 (0.06)	2.91–3.12	<b>4.75</b>	0.011 (0.009)	
	Mn-Mn	3.13 (0.01)	3.12–3.14	<b>1.5</b>	0.007 (0.005)	
	Mn-Mn	3.48 (0.04)	3.46–3.52	<b>1.5</b>	0.007 (0.005)	
<b>4</b>	Mn-O	1.86 (0.04)	1.86–2.18	<b>2.25</b>	0.005 (0.004)	1.8
	Mn-O	2.08 (0.08)		<b>1.75</b>	0.010 (0.001)	$\Delta E_0 = -14.2$
	Mn-N	2.18 (0.12)	2.14–2.37	<b>1.75</b>	0.010 (0.001)	
	Mn-Mn	2.74 (0.10)	2.79	<b>0.5</b>	0.010 (0.001)	
	Mn-C	2.85 (0.10)		<b>5.5</b>	0.015 (0.001)	
	Mn-Mn	3.10(0.05)	3.13–3.18	<b>1.5</b>	0.004 (0.003)	
	Mn-Mn	3.66 (0.13)	3.46, 3.63	<b>1.0</b>	0.009 (0.001)	
<b>5</b>	Mn-O	1.90 (0.02)	Mn-O:	<b>3.75</b>	0.006 (0.001)	0.2
			1.85–2.36			
	Mn-N/O	2.12 (0.04)	Mn-N:	<b>2.25</b>	0.014 (0.005)	
			2.03–2.04			
	Mn-Mn	2.81 (0.03)	2.77–2.87	<b>1.5</b>	0.005 (0.002)	
Mn-C	2.95 (0.04)	2.82–3.03	<b>3.5</b>	0.008 (0.010)		
Mn-Mn	3.24 (0.02)	3.20–3.23	<b>1.5</b>	0.004 (0.001)		
<b>6</b>	Mn-O	1.87 (0.01)	Mn-O:	<b>4.25</b>	0.005 (0.001)	0.7
			1.85 – 2.20			
	Mn-O/N	2.11 (0.01)	Mn-N:	<b>1.75</b>	0.020 (0.012)	
2.03 – 2.05						
Mn-Mn	2.83 (0.05)	2.76–3.07	<b>3</b>	0.007 (0.001)		

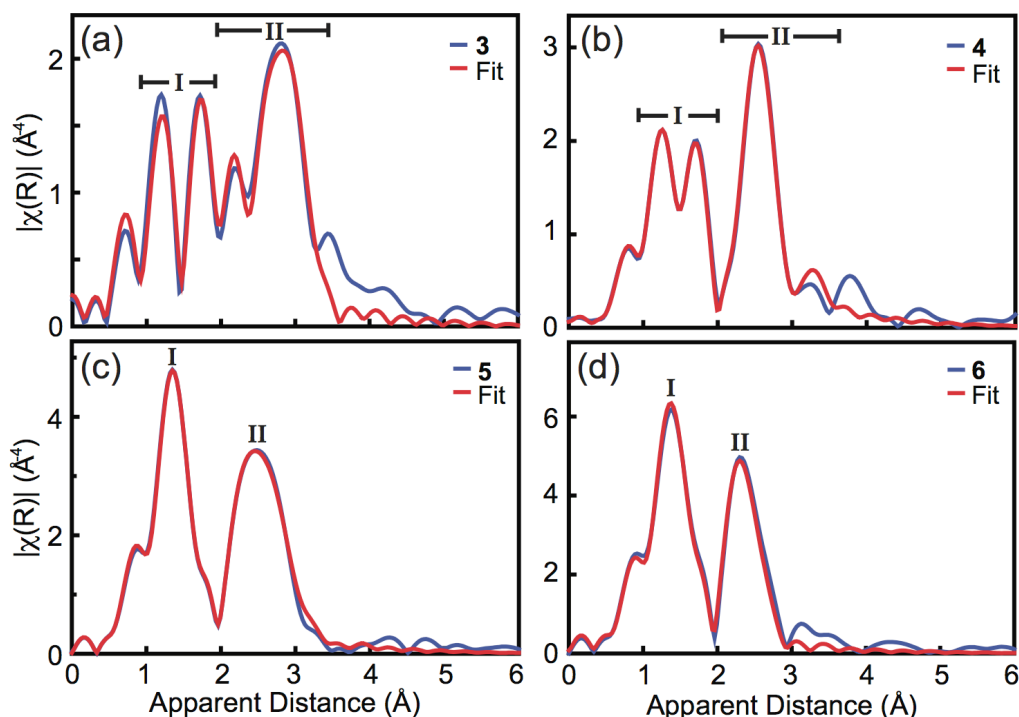
<sup>a</sup> Complex **3** was fit in the k-range of  $2.0 < k$  (1/Å)  $< 11.0$  ( $1.0 < R$  (Å)  $< 3.5$ ). Complex **4** was fit in the k-range of  $2.0 < k$  (1/Å)  $< 11.0$  ( $1.0 < R$  (Å)  $< 4.0$ ). Complex **5** was fit in the k-range of  $2.2 < k$  (1/Å)  $< 11.0$  ( $1.0 < R$  (Å)  $< 3.0$ ). Complex **6** was fit in the k-range of  $2.1 < k$  (1/Å)  $< 11.4$  ( $1.0 < R$  (Å)  $< 3.3$ ).

Figure S8 shows the Fourier transform (FT) of the  $k^3$ -weighted Mn EXAFS and corresponding fits for these complexes. All FT peaks occur at an apparent distance ( $R'$ ), which is shorter than the actual interaction distances ( $R$ ) by  $\sim 0.5$  Å due to the scattering phase shift. The shoulder peak occurring below  $R' = 1$  Å arises from incomplete background removal.

For complexes **3** and **4** (Figure S8, a and b), the FT features can be separated into two regions described as metal-ligand interactions (region I,  $1 \text{ Å} < R' < 2 \text{ Å}$ ) and mixed metal-metal/metal-ligand interactions (region II,  $2 \text{ Å} < R' < 3.5 \text{ Å}$ ). Due to the close proximity of the Mn-C and Mn-Mn interactions in these two complexes ( $\sim 2.9$ - $3.1$  Å and  $\sim 3.1$  Å, respectively), it was necessary to include Mn-C interaction distances in order to obtain reasonable fitting results for complexes **3** and **4**.

In contrast, the requirement for including Mn-C interactions in the FT fits for complexes **5** and **6** (Figure S8, c and d) was less obvious due to smeared scattering distributions. In these complexes, the Mn-C distances varied and their contributions to the EXAFS spectra were smaller relative to that for complexes **3** and **4**. For complex **5**, peaks I and II can be described as metal-ligand and mixed metal-ligand/metal-metal interactions, respectively. Peak I contains Mn-O and Mn-O/N contributions at  $\sim 1.9$  and  $\sim 2.1$  Å, and peak II consists of Mn-Mn ( $\sim 2.8$  and  $\sim 3.2$  Å) and Mn-C ( $2.9$ - $3.0$  Å) interactions. For complex **6** (Figure S8d), peak I corresponds to metal-ligand interactions and peak II corresponds to metal-metal interactions. The metal-ligand distances for Mn-O and Mn-O/N were resolved at  $\sim 1.9$  and  $\sim 2.1$  Å, respectively; and the Mn-Mn interactions

were approximated to  $\sim 2.8$  Å in peak II. These agree well with the average XRD distances summarized for **6** in Table 1.



**Figure S8** Fourier transforms of the Mn EXAFS for complexes **3-6** (blue) with fits (red). The EXAFS curve-fitting parameters are summarized in Table S1.

### EPR Methods

Perpendicularly polarized CW X-band (9 GHz) spectra were collected using a Bruker model E-500 spectrometer equipped with a super-high Q resonator (SHQE). Parallel polarized CW X-band (9 GHz) spectra were collected using a dual-mode cavity (ER 4116DM). All CW X-band spectra were collected under non-saturating slow-passage conditions. Temperature control was maintained with an Oxford Instruments model ESR900 helium flow cryostat with an Oxford ITC 503 temperature controller.

For complex **6**, using the coupling scheme  $S_A S_C S_{AC} S_B S_D S_{BD} S_{ACBD}$ , the energy levels can be calculated using this formula:<sup>8</sup>

$$\begin{aligned}
 H = & -J_{33} [S_{AC}(S_{AC} + 1) - S_A(S_A + 1) - S_C(S_C + 1)] \\
 & -J_{44} [S_{BD}(S_{BD} + 1) - S_B(S_B + 1) - S_D(S_D + 1)] \\
 & -J_{34} [S_{ACBD}(S_{ACBD} + 1) - S_{AC}(S_{AC} + 1) - S_{BD}(S_{BD} + 1)]
 \end{aligned}$$

Using the J values obtained from magnetic susceptibility data (Table 2), we expect that complex **6** has a ground spin state of  $S_{ACBD} = 1$  ( $S_{AC} = 4, S_{BD} = 3$ ), and the first excited state is  $S_{ACBD} = 2$  ( $S_{AC} = 4, S_{BD} = 2$ ). We cannot ascertain which state is giving rise to the low-temperature EPR signal centered at 330 mT as we find acceptable simulations for the centermost feature using either  $S = 1$  or  $S = 2$  as the ground state spin quantum number. The additional spectral intensity at 270 and 400 mT in the experimental 5 K spectrum is not accounted for in our simulations. The

temperature-dependent data show that these features results from transitions between levels of higher spin states that become more populated at elevated temperatures (see Figure 4).

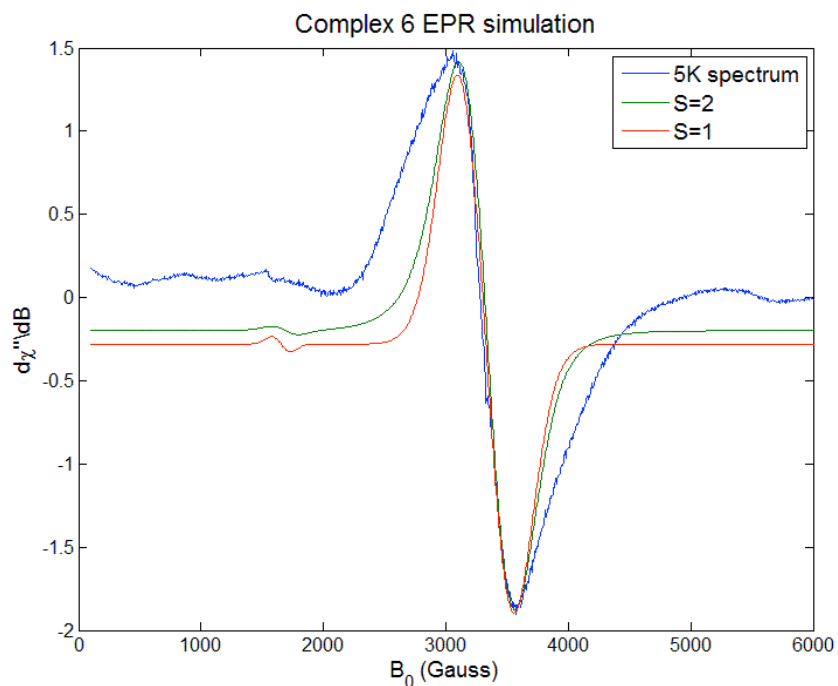


**Figure S9.** X band (9.33 GHz) CW EPR of complex **6** acquired at 5 K (blue trace). Simulations are presented for  $S = 1$  and  $S = 2$  ground states. Simulation parameters: (red trace)  $S = 1$ ,  $g = 2$ , zero-field splitting  $D = 1000$  MHz,  $E/D = 0.1$ ; (green trace)  $S = 2$ ,  $g = 2$ , zero-field splitting  $D = 600$  MHz,  $E/D = 0.1$ . Simulations were performed using Matlab R2011b and the EasySpin 4.5.0 package.<sup>9</sup>

### Magnetism Studies

**General Considerations.** DC magnetic susceptibility measurements were carried out in the Molecular Materials Research Center in the Beckman Institute of the California Institute of Technology on a Quantum Design MPMS instrument running MPMS MultiVu software. Powdered samples (0.040–0.059 g) were fixed in eicosane (0.10–0.12 g) in gelatin capsules or in plastic wrap and suspended in clear plastic straws. Data were recorded at 0.5 T from 4–300 K. Diamagnetic corrections were made using the average experimental magnetic susceptibility of  $\mathbf{H}_3\mathbf{L}$  at 0.5 T from 100–300 K ( $-593 \times 10^{-6}$  cm<sup>3</sup>/mol) in addition to the values of Pascal's constants for amounts of solvent quantified for each sample using elemental analysis.

For compounds **6**, the  $\chi_M T$  data taken at 0.5 T were fit to the magnetic susceptibility equation derived from the isotropic spin Hamiltonian for three coupling constants,  $J_{34}$ ,  $J_{33}$ , and  $J_{44}$ . Specifically, the manganese centers were modeled as an asymmetric tetrahedron (Figure S9), with the basal three manganese centers ( $\text{Mn}_B$ ,  $\text{Mn}_C$ , and  $\text{Mn}_D$ ) modeled as an isosceles triangle. The exchange interactions between the apical  $\text{Mn}^{\text{III}}$  center ( $\text{Mn}_A$ ) and the two  $\text{Mn}^{\text{IV}}$  centers ( $\text{Mn}_B$ ,  $\text{Mn}_D$ ),  $J_{34}$ , were assumed to be the same as the interactions between the  $\text{Mn}^{\text{IV}}$  centers and the basal  $\text{Mn}^{\text{III}}$  ( $\text{Mn}_C$ ) in order to allow the eigenvalues to be determined for the isotropic spin Hamiltonian [Eq. (1)].

$$\hat{H} = -2J_{34}[(\hat{S}_A \cdot \hat{S}_B) + (\hat{S}_A \cdot \hat{S}_D) + (\hat{S}_B \cdot \hat{S}_C) + (\hat{S}_C \cdot \hat{S}_D)] - 2J_{33}(\hat{S}_A \cdot \hat{S}_C) - 2J_{44}(\hat{S}_B \cdot \hat{S}_D) \quad (1)$$

The eigenvalues were determined using the Kambe method.<sup>10</sup> The data were fit from 10–300 K using Matlab<sup>11</sup> by minimizing  $R = \sum |(\chi_M T)_{obs} - (\chi_M T)_{calcd}|^2 / \sum (\chi_M T)_{obs}^2$ . Similar models were used to fit the 0.5 T  $\chi_M T$  data taken of compound **3** and **4** with the concomitant change in oxidation states at the Mn centers (Figure S9). The Hamiltonian for **3** and **4** is Eq. (2), although note the different locations of the Mn<sup>II</sup> centers and Mn<sup>III</sup> centers.

$$\hat{H} = -2J_{23}[(\hat{S}_A \cdot \hat{S}_B) + (\hat{S}_A \cdot \hat{S}_D) + (\hat{S}_B \cdot \hat{S}_C) + (\hat{S}_C \cdot \hat{S}_D)] - 2J_{22}(\hat{S}_A \cdot \hat{S}_C) - 2J_{33}(\hat{S}_B \cdot \hat{S}_D) \quad (2)$$

For compound **5**, the  $\chi_M T$  data taken at 0.5 T were fit to the magnetic susceptibility equation derived from the isotropic spin Hamiltonian for two coupling constants  $J_{TOP}$  and  $J_{BOT}$ . The Mn centers were modeled as an equilateral triangle interacting with a fourth metal center (Figure S9, right). The resulting Hamiltonian is Eq. (3). The eigenvalues were determined using the Kambe method.<sup>10</sup> The data were fit from 10–300 K using Matlab<sup>11</sup> by minimizing  $R = \sum |(\chi_M T)_{obs} - (\chi_M T)_{calcd}|^2 / \sum (\chi_M T)_{obs}^2$ .

$$\hat{H} = -2J_{TOP}[(\hat{S}_A \cdot \hat{S}_D) + (\hat{S}_B \cdot \hat{S}_D) + (\hat{S}_C \cdot \hat{S}_D)] - 2J_{BOT}[(\hat{S}_A \cdot \hat{S}_B) + (\hat{S}_B \cdot \hat{S}_C) + (\hat{S}_A \cdot \hat{S}_C)] \quad (3)$$

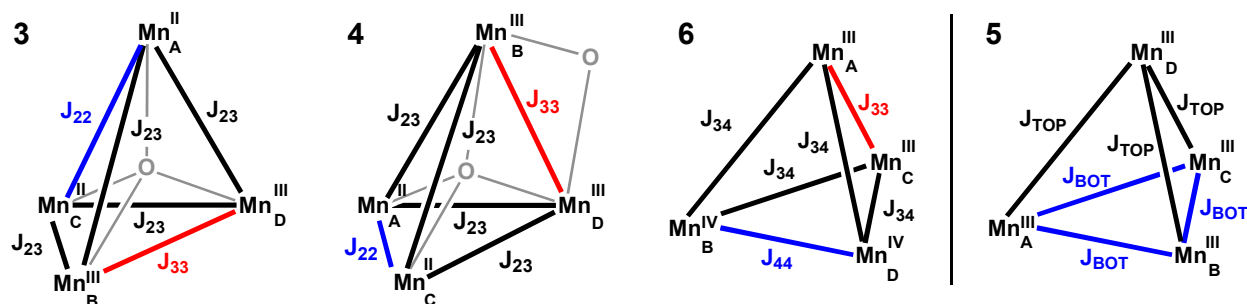


**Figure S10.** Exchange coupling models employed for **3-6**. For complexes **3** and **4**, the oxido ligands are shown in gray. In all cases, the Mn<sub>4</sub> tetrahedra are drawn such that the ligand framework L<sup>3-</sup> is below the drawing (as in Scheme 1).

### Crystallographic Information

**Table S2.** Crystal and refinement data for complexes **2, 3, 4**, and **7**.

	<b>2</b>	<b>3</b>	<b>4</b>	<b>7</b>
empirical formula	C <sub>65</sub> H <sub>51</sub> N <sub>6</sub> O <sub>12</sub> Mn <sub>4</sub> • 0.66(C <sub>4</sub> H <sub>10</sub> O)• C <sub>3</sub> H <sub>7</sub> N• 0.43(H <sub>2</sub> O)	0.59[C <sub>64</sub> H <sub>48</sub> F <sub>3</sub> N <sub>6</sub> O <sub>13</sub> SMn <sub>4</sub> ] <sup>+</sup> 0.41[C <sub>65</sub> H <sub>51</sub> N <sub>6</sub> O <sub>12</sub> Mn <sub>4</sub> ] <sup>+</sup> [CF <sub>3</sub> O <sub>3</sub> S] <sup>-</sup>	C <sub>63</sub> H <sub>48</sub> N <sub>6</sub> O <sub>11</sub> Mn <sub>4</sub> • 3(C <sub>3</sub> H <sub>7</sub> NO)	C <sub>72</sub> H <sub>61</sub> F <sub>3</sub> Mn <sub>4</sub> N <sub>10</sub> O <sub>14</sub> S• C <sub>6</sub> H <sub>6</sub>
formula wt	1456.92	1529.34	1504.12	1671.19
T (K)	100(2)	100(2)	100(2)	100(2)
a, Å	19.5671(8)	12.3050(6)	12.6007(5)	15.410(3)
b, Å	12.5184(5)	15.5248(7)	13.0991(5)	24.640(5)
c, Å	27.8828(11)	37.6815(18)	20.5699(8)	19.230(4)
α, deg	90	90	99.263(2)	90
β, deg	106.461(2)	98.567(3)	95.161(2)	103.16(3)
γ, deg	90	90	94.247(2)	90
V, Å <sup>3</sup>	6549.9(5)	7118.1(6)	3323.8(2)	7110(2)
Z	4	4	2	4

cryst syst	Monoclinic	Monoclinic	Triclinic	Monoclinic
space group	P 2 <sub>1</sub> /c	P 2 <sub>1</sub> /n	P-1	P 2 <sub>1</sub> /n
d <sub>calcd</sub> , g/cm <sup>3</sup>	1.477	1.427	1.503	1.561
θ range, deg	1.96 to 28.34	1.68 to 27.50	1.63 to 30.62	1.40 to 31.33
μ, mm <sup>-1</sup>	0.826	0.819	0.817	0.807
abs cor	None	None	None	Empirical
GOF	1.086	1.136	1.542	1.640
R1, <sup>a</sup> wR2 <sup>b</sup> (I > 2σ(I))	0.0643, 0.1784	0.0848, 0.2042	0.0536, 0.0634	0.0572, 0.1694

<sup>a</sup> R1 =  $\sum ||F_o| - |F_c|| / \sum |F_o|$ . <sup>b</sup> wR2 =  $\{ \sum [w(F_o^2 - F_c^2)^2] / \sum [w(F_o^2)^2] \}^{1/2}$ .

### Special Refinement Details

Refinement of F2 against ALL reflections. The weighted R-factor (wR) and goodness of fit (S) are based on F2, conventional R-factors (R) are based on F, with F set to zero for negative F2. The threshold expression of  $F2 > 2\sigma(F2)$  is used only for calculating R-factors(gt) etc. and is not relevant to the choice of reflections for refinement. R-factors based on F2 are statistically about twice as large as those based on F, and R-factors based on ALL data will be even larger.

All esds (except the esd in the dihedral angle between two l.s. planes) are estimated using the full covariance matrix. The cell esds are taken into account individually in the estimation of esds in distances, angles and torsion angles; correlations between esds in cell parameters are only used when they are defined by crystal symmetry. An approximate (isotropic) treatment of cell esds is used for estimating esds involving l.s. planes.

### Compound 2

Crystals were mounted on a glass fiber using Paratone oil then placed on the diffractometer under a nitrogen stream at 100K.

The acetate bridging Mn3-Mn4 adopts two bridging modes, one mode is the usual  $\kappa^2(O)$  mode as in the other acetates and the other with a single oxygen atom forming the bridge. Both orientations were refined with geometric restraints based on similar ligands in the model. The diethyl ether solvent was refined with geometric restraints, a fixed temperature factor and variable occupancy. No restraints were placed on the DMF. The lone oxygen (presumably water) was refined with a fixed temperature factor and a variable occupancy. The similar ADP and rigid-bond restraints were used on C2C.

### Compound 3

Crystals were mounted on a glass fiber using Paratone oil then placed on the diffractometer under a nitrogen stream at 100K.

The electron density map of the solvent area in this crystal contains a very clearly defined triflate anion and another long ill-defined chain of density, presumably arising from disordered hexane/dimethoxyethane solvents. This latter was solvent flattened using the program SQUEEZE.<sup>7</sup> The total potential solvent is 1203Å<sup>3</sup>, about 17% of total unit cell volume, which required 315 electrons to adjust the observed intensities such that this area contained no electron density. This is reasonably consistent with two hexane molecules per asymmetric unit.

The trifluoromethanesulfonate anion coordinating Mn4 has compositional disorder with an acetate anion, with populations at 59% and 41%, respectively. The acetate was modeled isotropically. The similar ADP and rigid-bond restraints were used on C64 and O8.

### Compound 4

Crystals were mounted on a glass fiber using Paratone oil then placed on the diffractometer under a nitrogen stream at 100K.

The non-bridging acetate bound to Mn4 is disordered over two orientations.

#### Compound 7

Crystals were mounted on a plastic loop using Paratone oil then placed in liquid N<sub>2</sub> for transport to SSRL beamline 12-2.

A molecule of benzene (the crystallization solvent) was found in the lattice and could not be satisfactorily modeled anisotropically. It was thus modeled isotropically and hydrogens were not calculated for this molecule.

#### References

1. J. B. Vincent, H. R. Chang, K. Folting, J. C. Huffman, G. Christou and D. N. Hendrickson, *J. Am. Chem. Soc.*, 1987, **109**, 5703-5711.
2. H. Saltzman and J. G. Sharefkin, *Org. Synth. Coll.*, 1973, **5**, 658.
3. P. S. Bryan and J. C. Dabrowiak, *Inorg. Chem.*, 1975, **14**, 296-299.
4. J. S. Kanady, J. L. Mendoza-Cortes, E. Y. Tsui, R. J. Nielson, W. A. Goddard and T. Agapie, *J. Am. Chem. Soc.*, 2013, **135**, 1073-1082.
5. J. S. Kanady, E. Y. Tsui, M. W. Day and T. Agapie, *Science*, 2011, **333**, 733-736.
6. M. Newville, *J Synchrotron Radiat.*, 2001, **8**, 322-324.
7. B. Ravel and M. Newville, *J Synchrotron Radiat.*, 2005, **12**, 537-541.
8. A. G. Bencini, *Electron Paramagnetic Resonance of Exchange Coupled Systems*, Springer, Verlag, Berlin, 1990.
9. S. Stoll and A. Schweiger, *J Magn Reson*, 2006, **178**, 42-55.
10. K. Kambe, *J Phys. Soc. Japan*, 1950, **5**, 48-51.
11. *Matlab*, 7.10.0.499 (R2010a); The MathWorks, Inc., Natick, MA, 2010.